INTERNATIONAL JOURNAL OF
COASTAL & OFFSHORE ENGINEERING IJCOE Vol.6/No.5/ Autumn 2021 (1-9)/ **Special issue of "Marine Renewable Energy"**

Available online at http://www.ijcoe.org

The role of different positions of tidal turbines for energy extraction in Qeshm channel

Maryam Soyuf Jahromi[1*], Mahdieh Emami[2]

[1*] *Assistant Professor of physical oceanography, Department of Nonliving Resources of Atmosphere and Ocean, Faculty of Marine Science and Technology, University of Hormozgan, Bandar Abbas, Iran; oyufjahromi@yahoo.com.au*

[2] *PhD candidate of physical oceanography, Department of Nonliving Resources of Atmosphere and Ocean, Faculty of Marine Science and Technology, University of Hormozgan, Bandar Abbas, Iran; mahdiehemami94@yahoo.com*

ARTICLE INFO

Article History:
Received: 16 Nov. 2021
Accepted: 30 Nov. 2021

Keywords:
Energy extraction
Turbine
Khuran Strait
Tides
Mike3

ABSTRACT

The use of renewable energy instead of oil and gas reservoirs in the Persian Gulf can be a good platform for renewable energy farms. This study investigates the energy generated by the tidal flow velocity in the Qeshm channel, using a three-dimensional hydrodynamic model, MIKE3, Flow Model FM. By installing a hypothetical tidal turbine from Voith Company, with a diameter of 1 m at seven different stations of the model (respectively from east to west of the channel), the tidal energy from the horizontal flow of the area is calculated. In the mentioned simulation, wind stress and thermohaline flow are ignored so that the dominant current is the current caused by the change of water level due to the tide. The flow velocity pattern in spring and neap tides at Higher High Water (HHW) was then analyzed at the seven stations. The energies of the simulated currents showed that the east side of the channel had more energy potential on the days of spring tides, so that at IP1 station, in the first spring tide, 175 watts of electricity is generated, which in the second spring tides decreases by 28.5%. On the other hand, the west side of the channel had the potential to generate electricity in neap tides. Station IP6 had the potential to generate electricity in both the spring and neap tides, which had more neap tides potential than the spring tides. The difference in power generated in the first and second neap tides at IP6 was only 0.7%, which is less than 30.2 W compared to the first and second spring tides. Therefore, it can be said that according to the shape of the region, the second bend of Qeshm channel was a more suitable place for energy extraction with the assumed tidal turbine in the region.

1. Introduction

One of the most important ways to use renewable energies is the use of the seas energies. Using seas to receive energy has attracted attentions of the international community after the oil crisis of the 1970s. Marine Renewable Energies (here after MRE) have the ability to provide 7% of global electricity demand [1]. Among all MRE, the tidal current energies are due to the tides, resulting the gravitational pull of the moon [2][3]. Tidal energy is one of the most reliable and promising energy sources [4], due to its predictability and many other attractive features [5]. It can also reduce reliance on fossil fuels. Tidal energy is expressed both as the kinetic energy of tidal currents and as potential energy of the water level difference between the tides.

The flows of tides in tidal channels are particularly important, especially in places where the density difference and wind-driven flows (as the other two types of marine currents; [6] are insignificant. Moreover, the flow pattern can be locally affected by shoreline shape and depth changes [7]. Therefore, identifying the best place to install tidal current turbines will be one of the challenging issues in the MRE basin. In this regard, countries such as China (e.g. [3]), the European Union (e.g. [8], the United Kingdom (e.g. [9], and other developed countries, have conducted researches in this field in order to take a step towards economic savings of this type of renewable energy. Few researches have been done in Iran [10][11][12] that deal with these issues. In this study, the Qeshm tidal channel, located in the north of the Strait of Hormuz, which is strongly affected by the tides [13][14], has been simulated to identify the location of the maximum tidal flow velocity in the channel. Then, the best place to receive tidal energy is calculated by

assumptive tidal turbines in different selected positions along Qeshm channel.

2. Materials and Methods

2.1. The study area

The studied area was the Qeshm tidal channel (Figure 1, 26.66-27.15°N, 55.23-56.27°E), located in the north of the Strait of Hormuz, Persian Gulf (24-30°N, 48-56°E). Persian Gulf is a semi-closed basin [16] with a length of 990 km, a width of 56-338 km, and an average depth of 35 m [17][18]. It is located in the southwest of Asia on a continental shelf. The Persian Gulf is connected to the Oman Sea and the Indian Ocean by the Strait of Hormuz and is surrounded by Iran, Iraq, Kuwait, Saudi Arabia, Bahrain, Qatar, and the United Arab Emirates.

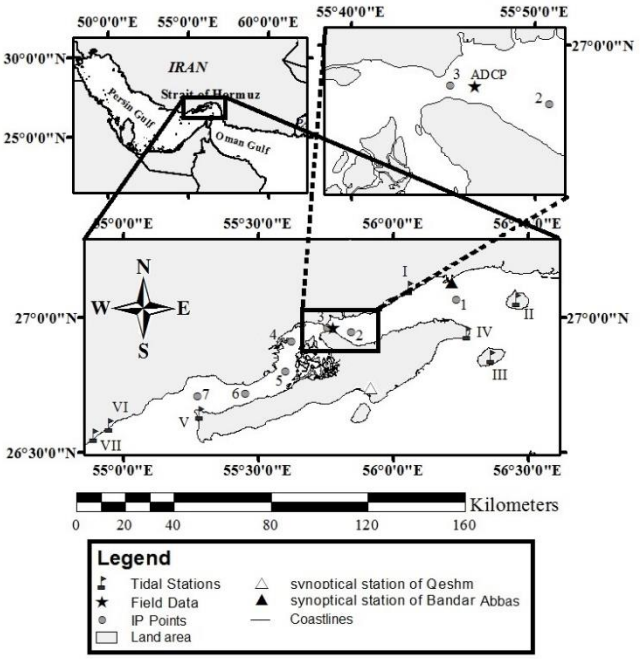

Figure 1. Geographical location of Qeshm channel relative to Persian Gulf. Stations 1 to 7 are the position of model outputs along the channel to determine the maximum tidal velocity of the channel. Stations I to VII are tidal stations. The triangles are meteorological stations and the star is the location of ADCP. This figure is prepared in ArcGIS [15] environment.

The Strait of Hormuz is also a curved waterway (Figure 1) that separates the Iranian plate from the Arabian plate and connects Persian Gulf to Oman Sea. The bottom of Strait of Hormuz has a steep slope in the north-south direction. This strait is internationally strategic and the countries of its border produce 30% of the world's oil which is exported through the Strait of Hormuz. In addition to oil, 45% of the world's natural gas reserves are held by the region countries [19]. The existence of oil has led to the economic dependence of countries in the region on oil, and therefore in the field of MRE, no serious action has been taken by countries of the region [20]. Qeshm Island, is the largest island of Persian Gulf with an area of 2.5 times the country (island) of Bahrain [21] in the Strait of Hormuz. Qeshm channel is located between the north of Qeshm Island and the south coast of Iran. This channel is also sometimes called the Khuran Strait (Figure 1). This channel is also known by its eastern important ports (Shahid-Rajai and Bahonar port) and its western aquatic environment (mangrove forests) near IP4 of Figure 1 and it has unique complexities.

Although the length of the Persian Gulf from the Strait of Hormuz to the northwestern part of Arvand River (with discharge of 435 m^3s^{-1}, [22]) is approximately 1000 km [23][24], but the length of the Qeshm channel is about 110 km [25]. The maximum width of the channel is 25 km between Bandar Abbas and Qeshm city and the minimum width of the channel is 3.5 km between the Pohl port and Laft port in the Khuran Strait [25].

The Persian Gulf's climate is affected by extra-tropical weather system, which comes from the northwest. On the other side, the Oman Sea is affected by the tropical system of the Arabian Sea and the Indian Ocean, so that the monsoon cycle causes south winds in summer and strong north winds in winter. The Strait of Hormuz is the border of these two climate systems [18], which modulates the effects of those two systems; so that the prevailing wind is local and short-lived duration. Hence, the Qeshm channel is more affected by tides [25] than the prevailing climatic patterns. The Qeshm channel tides are mixed semidiurnal tides and affected by K_1, N_2, S_2, M_2, and O_1 components [26][27][28]. Since Qeshm channel is affected by the shape of its coastline [29], then the natural characteristics can affect the placement of devices in energy extraction.

2.2. The simulation method

To study the Qeshm channel MRE, the three-dimensional hydrodynamic model MIKE 3 [30], Service Pack 3, 2012 version, related to the Danish Hydraulic Institute (DHI) has been used, which has already been used in other aquatic basin studies (such as [31], [30], [32], [33], [34]). Besides, the models of this institute have been already tested in the Qeshm channel area (for example [35], [36], [37] and [29]). The MIKE 3 flow model, abbreviated MIKE 3 FM, hereinafter referred to MIKE, uses the finite volume method. This hydrodynamic module solves the three-dimensional equations of stability, mass, and time-dependent momentum, the incompressibility of Navier-Stokes equations using the Boussinesq approximation and the hydrostatic pressure. MIKE uses the UNESCO equations for seawater state (1980) [38] in the form of a series of relationships between salinity, temperature, and density [39]. Its most important feature is the flexible triangular and rectangular grid with different sizes in its computational range [40], which it is used a triangular grid in this study (Figure 2). Figure 2 shows the details of grids and bathymetry of the Qeshm channel, prepared in the MIKE Zero. Numbers of created triangular grids were 4433 with 3136 points. The topographic information of the area is provided by

NOAA NGDC and provided by ERDDAP Server [41]. The main source of NOAA NGDC data is the ETOPO1 satellite, which is made up of multiple regional and global datasets and connects the data with an alternative global model of the land surface, land topography, and ocean bathymetry.

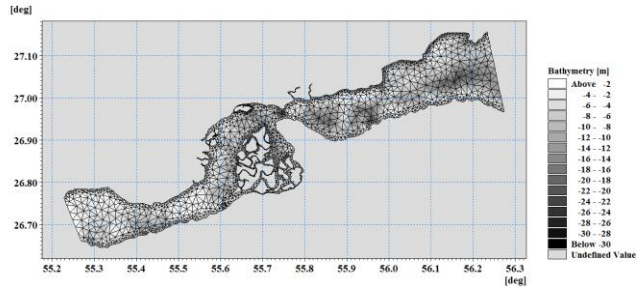

Figure 2. The bathymetry of Qeshm channel with the flexible triangular mesh scheme of the model in MIKE3.

The used coordinate system for the simulation was the Cartesian coordinate system in horizontal directions, and the Sigma coordinate system in the vertical direction, so that the vertical coordinates could follow the elevation of the bed. The numbers of layers of the Sigma coordinate system were considered five levels, which was appropriate due to the shallow depth of the area (with maximum depth of -30 m). The thickness of each layer varies from at least 0.4 m to 6 m (depending on bed depths and changes of water levels in spring and neap tides).

Two land (hard) borders in the north and the south of domain and two open borders in the east and the west were considered (Figure 2) where the open borders could change the water level due to tides. The length of the channel was 110 km and its width was 19.8 km in the eastern border and 11 km in the western border with the maximum depth of -30 m. Tidal data were used on the open borders. Table 1 shows the location of tidal stations around the Qeshm channel (flags I to VII of Figure 1). It was used the stations of I and VI for tidal injection into the simulation.

Table 1. Tidal stations on the domain.

No.	Station Name	Location	
		Latitude (˚N)	Longitude (˚E)
I	Bandar-E Shahid Rajai	27.11093415	56.0605717
II	Hormuz Island	27.0678342	56.46119855
III	Larak	26.85571385	56.36407975
IV	Bandar-E Bahman	26.9455038	56.2775832
V	Basaidu	26.6447722	55.2829242
VI	Bandar Lengeh	26.5640657	54.8908389
VII	Bandar Kong	26.6028576	54.94731545

Since the location of Qeshm channel is almost horizontal, narrow, and long and because of small variations of its latitude (26.6ºN-27.2ºN, with the width of approximately about 0.8 degrees), it does not cause much deviation in the Coriolis parameter. Maximum changes in the Coriolis parameter are less than one percent (0.45%). Therefore, the changes of the Coriolis force can be ignored in the current simulation.

Maximum wind speed and direction information, in two synoptical stations of Bandar Abbas (27.13ºN and 56.22ºE and 9.8 m above sea level [42], black triangle on Figure 1) and Qeshm (26.73ºN and 55.91ºE and 6 m above sea level, white triangle on Figure 1) were extracted from the Meteorological Organization of Iran in January 2016. Figure 4 shows these data in Matlab software [43]. It can be seen that the two meteorological stations are slightly different from each other. The average wind speed of Qeshm station is 5.80±2.31 m/s (mean ± standard deviation) and Bandar Abbas station is 5.67±1.71 m/s (mean ± standard deviation). Therefore, due to the small size of Qeshm channel, the wind speed can be considered constant and equals to 5.74 m/s in the whole domain. To simplify the simulation, the wind speed was considered to be zero, which was previously assumed in the study of [25]. The wind patterns are also local, so it is reasonable to consider the wind speed equals with zero. Therefore, it was assumed that wind stresses of the basin are negligible (according to the study of [25]) and equal to zero. It was also assumed that the current due to the density difference does not have much effect on the channel (according to the study of [25]) and the current caused by the waves has not been considered. As a result, it was assumed that the current pattern of Qeshm channel in this simulation were effected by tides.

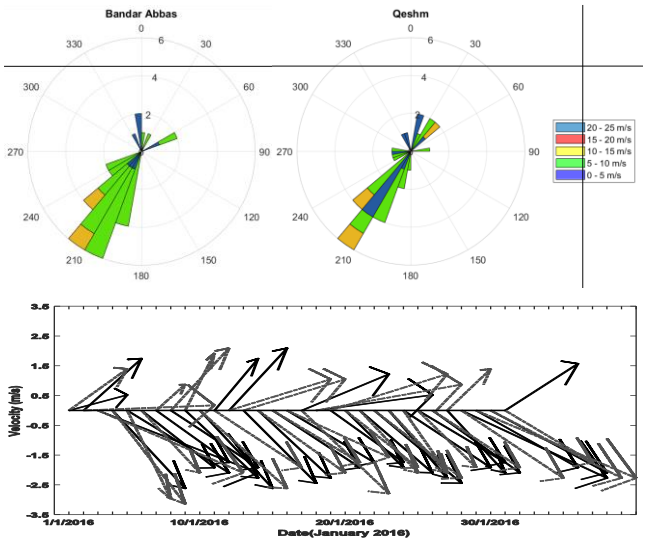

Figure 3. Comparison of wind speed between two synoptical stations of Bandar Abbas (black triangle of Figure 1) and Qeshm (white triangle of Figure 1), in January 2016. Up) Wind rose of Bandar Abbas and Qeshm. Down) The same feather diagram, for Bandar Abbas (black solid line) and Qeshm (gray dash line).

The simulation outputs included the flow speed and direction along horizontal and vertical directions, the velocity components along x, y and z axes. For the longitudinal check of Qeshm channel, seven stations (IP1 to IP7 of Table 2) were selected to study outputs quantitatively. These stations are shown on Figure 1 as gray points numbered one to seven. In each station it was installed an assumptive turbine.

Table 2. Location of turbines on the studied area as illustrated on Figure 1.

Station names	Geographical location	
	Latitude (˚N)	Longitude (˚E)
IP 1	27.06656	56.23585
IP 2	26.94609	55.84574
IP 3	26.9633	55.75624
IP 4	26.91282	55.622
IP 5	26.80152	55.6002
IP 6	26.71891	55.45219
IP 7	26.70973	55.27549

The appropriate input data is a good way to achive a good simulation. And then the model was run for one month (January, 2016) and the model outputs were extracted in the stations mentioned on Table 2 in spring and neap tides (Table 3).

Table 3. Spring and neap tides of the model

Date (year/m/d)	Time (hour)	Tidal type		Model time step
2016/1/2	1:00	1st Neap	HHW*	24
	7:00		HLW+	30
	13:00		LHW**	36
	19:00		LLW++	42
2016/1/11	4:00	1st Spring	HLW	243
	10:00		LHW	249
	16:00		LLW	255
	22:00		HHW	261
2016/1/18	3:00	2nd Neap	LHW	410
	9:00		HLW	416
	15:00		HHW	422
	22:00		LLW	429
2016/1/26	4:00	2nd Spring	LLW	603
	10:00		LHW	609
	16:00		HLW	615
	22:00		HHW	621

*HHW stands for Higher High Water
+LHW stands for Lower High Water
**HLW stands for Higher Low Water
++LLW stands for Lower Low Water

To extract the most suitable water level data for open boundaries, it was used Tidal Model Driver, hereafter TMD package version 2005 [44], related by Oregon State University [45] in Matlab software [43]. This software was written by Oregon State University in 2003 and was used in other studies such as [46]. This package can predict tides by the accuracy of at least one minute by one minute at any various point of the whole world. It was used the tidal amplitudes and phases of the eight main components (M2, S2, N2, K2, K1, O1, P1, Q1) of Persian Gulf on the special Persian Gulf version of TMD package by the resolution of 30 seconds on 30 seconds in January 2016 [47][48].

The reason of using TMD package was good accuracy on the field measurement comparisons. Figure 4 is a sample comparison (in January 2016) between TMD model (solid lines) and the field Iran National Cartographic Center water levels data in an eastern station (Bandar Abbas, Figure 4, up) and a western station (Bandar Lengeh, Figure 4, down) of open boundaries (dot lines). It is obvious that TMD can predict roughly accurate tidal information. This is obvious from the comparisons of measured data of all stations of Table 1 with TMD and tidal information of Tides4fishing website [49].

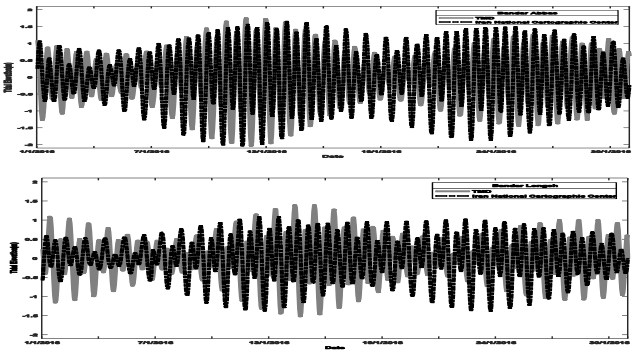

Figure 4: Comparison of model input data achieved by TMD (solid lines) and Iran National Cartographic Center field data (dot lines) in (up) eastern and (down) western boundaries in January 2016.

In order to force MIKE3 by tidal inputs of open boundaries, the average of four eastern station (I, II, III and IV of Table 1) was used for eastern boundary and the average of three western stations (V, VI and VII of Table 1) were used for western boundary of Qeshm channel. Their means were respectively 1.68 m and 2.03 m on the eastern and western boundaries. To import tidal data to MIKE3, it was used the middle of each eastern and western boundary.

To calibrate and validate MIKE3 model, measured ADCP current speed (located 26.963°N and 55.779°E) at depth 13 m from the bed near the Qeshm channel narrowing (Figure 1, star point) by one-hour interval from 1 September 2005 to 11 September 2005 was compared with model (Figure 5) by two different tidal inputs of TMD and Tides4fishing website. These tidal data were entered into the open east and west boundaries of the MIKE3 model, as times series, with the extension of dfs0. Because each time-series data of the stations can be extracted and mapped for analysis and statistics at those stations and maps [51]. Then, the exact correct point of the field data (Figure 1, star point) was also defined in the model as an output. The horizontal tidal velocity described as:

$$U_h = \sqrt{u^2 + v^2} \quad (1)$$

where in Eq.(1), U_h stands for the horizontal tidal speed and u and v are horizontal components of tidal current in m/s.

The proper bed coefficient was also checked for the accuracy of results. In order to do that the model was implemented with the tide of 2005 and with different bed coefficients to compare the horizontal speed of the model sorted by different type of tides with the horizontal speed of the field data. From all tested and compared values of the bed coefficient of the model, the value of 0.004 was the most appropriate bed coefficient (Figure 5). As it is also obvious by the final outputs of MIKE3, there is better match between TMD input to the open boundaries of MIKE3 than Tides4fishing ones. Therefore, TMD was a better

choice as tidal boundaries inputs of MIKE3. Although, there is a phase difference of 2 and 3 hours with the ADCP data. Since the type of tides of area are semidiurnal by the period of 12 hours and 50 minutes, then this phase difference, is about 15-23%, and therefore it is roughly appropriate and acceptable.

For tidal energy, various formulas have been proposed. Here, it was used Eq.(2) which was previously studied by others (e.g. [52], [53], and [54]) as:

$$P_{TK} = -\frac{1}{2}\rho A\overline{U_A^3} \qquad (2)$$

where in Eq.(2) ρ stands for the flow density and is equal to 1025 kg/m^3 for the studied area [25]; A is the cross-section of the turbine in m^2, and U is the averaged fluid velocity achieved by the simulation in m/s. Since on different bed depths and at different tidal currents scales, different type of turbines can be used, then a small type of Pit turbine type has been selected from Voith company for this simulation. These turbines have a diameter of 0.80 to 8.40 m [55] and the diameter of the installed turbine in the model was considered equal to one meter.

The model included turbines and was run in January 2016 on Widows 8.1 Enterprise by a corei7 CPU, RAM of 8 GB and hard of 1 TB by time intervals of one hour. The times series of model velocity components on the exact time of Higher High Water, HHW, of each day, transferred to Microsoft office Excel [56] to achieve the horizontal velocity speed of the stations.

4. Results and Discussion

The horizontal speed of HHW in both neap and spring tides in January 2016 are stated in Table 4 and 5, respectively. The average surface horizontal speed of HHW in spring tides is 0.22 m/s (IP2 to IP6). This value is 0.17 m/s in neap tides. For bottom layer, these values decrease to 0.16 and 0.13 m/s in spring and neap tides respectively. It means that the average speed is higher at surface layer in compare with bottom layer in both spring and neap tides. As it is also obvious for all stations, the tidal horizontal flow speed trend is also the same for surface and bottom layers by reduced values of bottom layer.

Table 4. The calculated horizontal speed (in meters per seconds) at the stations (IP2 to IP6, Figure 1) of Qeshm channel at neap tides in January 2016.

Date	Station	The horizontal speed (m/s)		
		Surface layer	Bottom layer	Difference (Surface–Bottom) (%)
2nd January 2016 (1st Neap Tide)	IP2	0.13	0.10	2.90
	IP3	0.27	0.19	7.38
	IP4	0.14	0.11	3.27
	IP5	0.13	0.09	3.23
	IP6	0.26	0.20	6.76
	Average	0.19	0.14	4.71
18th January 2016 (2nd Neap Tide)	IP2	0.10	0.08	2.10
	IP3	0.19	0.15	4.60
	IP4	0.13	0.10	2.95
	IP5	0.12	0.10	1.23
	IP6	0.24	0.18	6.15
	Average	0.16	0.12	3.41

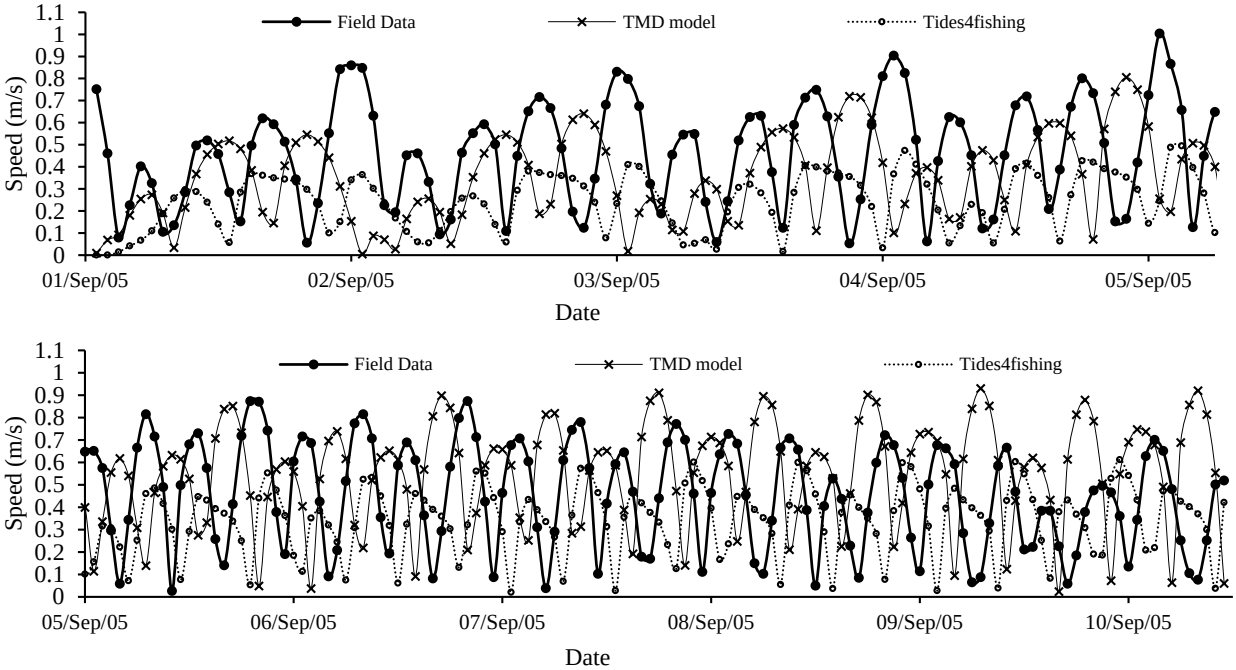

Figure 5. Comparison of MIKE3 current speeds (in meters per seconds) by different tidal input sources in September 1, 2005 to September 11, 2005. Tidal Model Driver input to MIKE3 are as solid line-cross points; Tides4fishing website [49] input to MIKE3 are as dot line-dot points and field data of [50] are as solid line-dot points.

Table 5. The calculated horizontal speed (in meters per seconds) at the stations (IP2 to IP6, Figure 1) of Qeshm channel at spring tides in January 2016.

Date	Station	The horizontal speed (m/s)		
		Surface layer	Bottom layer	Difference (Surface–Bottom) (%)
11th January 2016 (1st Spring Tide)	IP2	0.19	0.15	4.25
	IP3	0.37	0.26	10.42
	IP4	0.21	0.16	5.10
	IP5	0.17	0.13	4.03
	IP6	0.27	0.20	6.93
	Average	0.24	0.18	6.14
26th January 2016 (2nd Spring Tide)	IP2	0.16	0.12	3.49
	IP3	0.31	0.22	8.61
	IP4	0.16	0.12	3.72
	IP5	0.13	0.10	3.21
	IP6	0.25	0.19	6.40
	Average	0.20	0.15	5.09

Moreover, the average speed is higher on 1st and 2nd spring tides (0.24 and 0.20 for surface layer, and 0.17 and 0.15 for bottom layer, respectively). This amount is lower on 1st and 2nd neap tides (0.19 and 0.16 for surface layer, and 0.14 and 0.12 for bottom layer, respectively). At all stations (Table 4 and 5), the tidal horizontal speeds increase in both surface and bottom layers at spring tides while lower values are available for tidal speeds at neap tides.

Table 5 also shows that on the surface and bottom layers, the highest speeds referred to IP3 at the two spring tides (0.37 and 0.26 m/s during the first spring tide and 0.31 and 0.22 m/s during the second spring tide, respectively). It means that this station has potential for extract of tidal current energy. According to Table 5, the lowest values of surface and bottom layers referred to IP5 (0.17 and 0.13 m/s during the first spring tide and 0.12 and 0.10 m/s during the second spring tide, respectively) in the two spring tides (Table 5). Furthermore, in neap tides, IP6 has more high speed values on the surface and bottom layer (0.26 and 0.20 m/s at higher high water of the first neap tide and 0.24 and 0.18 m/s at HHW of the second neap tide, respectively) in compare with IP3 at the same time due to Table 4. It is also obvious that the horizontal speed of IP2 and IP5 both are small in neap tides and it means that these two stations are not suitable for extracting tidal current energy.

Therefore, results of Table 4 and 5 made clear that the positions of stations are important for high values of tidal horizontal speed (Eq. 2). The speed is low on IP2, the station before the narrowing part of the channel on the right of domain. Then it suddenly increases on IP3, the station exactly located on the first and most narrowing part of Qeshm channel. The IP3 speeds approximately doubles in compared with the previous station, IP2. Thereafter, the tidal horizontal speed decreases at IP4 before the mangrove forests and after the narrowest part of the channel. On IP5, after the mangrove forests, the horizontal tidal speeds decrease again and then increase again at the second narrowing part of the channel, IP6. This rhythm repeats by the period of 4 days between stations from IP2 to IP6.

On the other hand, as it is stated, there is a significant difference in station IP3 compared to IP2. The speed at station IP3 is almost twice that of IP2, which may be due to the difference in morphological characteristics of the location of station IP3 compared to IP2. This can reinforce the initial hypothesis about the effective location for extracting the most tidal energy.

Figure 6 shows the average tidal energy power in both the spring and the neap in January 2016 at each of the seven stations of Table 1.

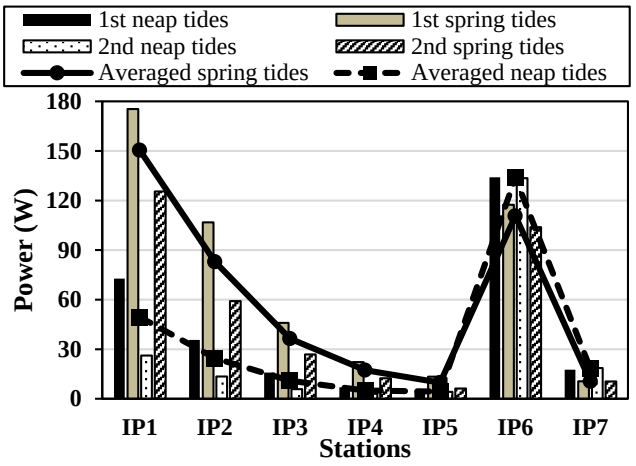

Figure 6. The averaged tidal energy powers (in watts) of turbines in January 2016 in spring and neap tides.

It can be seen that the highest tidal power is related to IP1 in the first spring tides (175.4 W) and then at the point IP6 in the first neap tides (134 W). Then, the first neap tides on IP6 and the second spring tides on IP1 are next with 125.5 and 133 watts, respectively. Relatively, the IP6 point has the most power among the stations at all four periods, with a maximum difference of 30 watts relative to each other. Station IP5 also has the lowest power between stations, which, due to its position after the middle curve of the channel, it makes sense to have the lowest tidal current velocity and therefore the lowest tidal energy. In general, except IP6 and IP7 stations, which have more power in neap tides, in other stations, the highest amount of power generation energy by the turbines are allocated to the days of the spring tides.

5. Conclusions

Results clearly showed that tidal velocities of Qeshm channel increased in both surface and bottom layers at the spring tides. It will be because of higher water levels of spring tides in compare with neap tides.

The model results of tidal current energy in Qeshm channel also illustrate that the location of the turbine installation is important. A spatial study of the highest power of installed turbines in different studied stations, showed well that the IP6 station has the highest amount of power generation capacity in both the spring and the neap tides, which according to the model results, it has

the highest flow velocity. Although the greatest depth, and of course the highest speed was near the Qeshm channel (IP3 station), the potential of IP6 station was more than IP3 station in both the spring and the neap tides at HHW.

It should be noted that in this study, only one turbine with the lowest cross section (turbine diameter) had been used in the simulations and calculations. Of course, in areas with more depth than the channel, turbines with more number and cross-section can be used to increase energy production capacity, which has the greatest depth near the narrowing part of the Qeshm channel.

List of Symbols

A	cross-section of the turbine [in m^2]
HHW	Higher High Water [in m]
HLW	Higher Low Water [in m]
LHW	Lower High Water [in m]
LLW	Lower Low Water [in m]
P_{TK}	Tidal energy power [in Watts]
u	The first horizontal component of tidal current [in m/s]
U_A	The averaged simulated fluid velocity for the turbine [in m/s]
U_h	The horizontal speed of tidal current [in m/s]
v	The second horizontal component of tidal current [in m/s]
ρ	density [in kg/m^3]

8. References

[1] Fox, C.J., Benjamins, S., Masden, E.A. and Miller, R., (2018), *Challenges and opportunities in monitoring the impacts of tidal-stream energy devices on marine vertebrates*. Renewable and Sustainable Energy Reviews, Vol.81, p.1926-1938.

[2] Sverdrup, K.A., Duxbury, A. and Duxbury, A.C., (2006), *Fundamentals of oceanography*. McGraw-Hill Higher Education.

[3] Liu, H.W., Ma, S., Li, W., Gu, H.G., Lin, Y.G. and Sun, X.J., (2011), *A review on the development of tidal current energy in China*. Renewable and sustainable energy reviews, Vol.15(2), p.1141-1146.

[4] Gu, Y.J., Lin, Y.G., Xu, Q.K., Liu, H.W. and Li, W., (2018), *Blade-pitch system for tidal current turbines with reduced variation pitch control strategy based on tidal current velocity preview*, Renewable Energy, Vol.115, p.149-158.

[5] Lee, J.H., Park, S., Kim, D.H., Rhee, S.H. and Kim, M.C., (2012), *Computational methods for performance analysis of horizontal axis tidal stream turbines*. Applied energy, Vol.98, p.512-523.

[6] Talley, L.D., (2011), *Descriptive physical oceanography: an introduction*. Academic press.

[7] Baker, C., (1991), *Tidal power*. Energy Policy, Vol.19(8), p.792-797.

[8] Magagna, D. and Uihlein, A., (2015), *Ocean energy development in Europe: Current status and future perspectives*. International Journal of Marine Energy, Vol. 11, p.84-104.

[9] Xia, J., Falconer, R.A. and Lin, B., (2010), *Impact of different operating modes for a Severn Barrage on the tidal power and flood inundation in the Severn Estuary*, UK. Applied Energy, Vol.87(7), p.2374-2391.

[10] Zabihian, F. and Fung, A.S., (2011), *Review of marine renewable energies: case study of Iran*. Renewable and Sustainable Energy Reviews, Vol.15(5), p.2461-2474.

[11] Rashid, A., (2012), *Status and potentials of tidal in-stream energy resources in the southern coasts of Iran: A case study*. Renewable and Sustainable Energy Reviews, Vol.16(9), p.6668-6677.

[12] Uihlein, A. and Magagna, D., (2016), *Wave and tidal current energy–A review of the current state of research beyond technology*. Renewable and Sustainable Energy Reviews, Vol.58, p.1070-1081.

[13] Sabbagh-Yazdi, S.R., Zounemat-Kermani, M. and Mastorakis, N.E., (2008), *Simulation wetting and drying of mangrove forests due to tidal currents in Qeshm canal*. International Journal of Mathematical Models and Methods in Applied Science, Vol.2(1) p.18-23.

[14] Sabbagh-Yazdi, S.R. and Zounemat-Kermani, M., (2009), *Numerical solution of tidal currents at marine waterways using wet and dry technique on Galerkin finite volume algorithm*. Computers and fluids, Vol.38(10), p.1876-1886. doi:10.1016/j.compfluid.2009.04.010

[15] ESRI, (2011), *ArcGIS Desktop*, 64-bit, Version 10.3, Released 2011, Redlands, CA: Environmental Systems Research Institute.

[16] Barth, H. J., and Khan, N. Y. (2008), *Biogeophysical setting of the Gulf.* In Protecting the Gulf's marine ecosystems from pollution, p.1-21. Birkhäuser Basel.

[17] Sheppard, C., Price, A. and Roberts, C., (1992), *Marine ecology of the Arabian region: patterns and processes in extreme tropical environments*. London, Academic Press.

[18] Reynolds, R.M., (1993), *Physical oceanography of the Gulf, Strait of Hormuz, and the Gulf of Oman—Results from the Mt Mitchell expedition*. Marine Pollution Bulletin, Vol.27, p.35-59.

[19] Cordesman, A.H., (2007), *Iran, oil, and the Strait of Hormuz*. Washington: Center for Strategic and International Studies. p.2-4.

[20] Al-Maamary, H.M., Kazem, H.A. and Chaichan, M.T., (2017), *Renewable energy and GCC States energy challenges in the 21st century: A review.* International Journal of Computation and Applied Sciences IJOCAAS, Vol.2(1), p.11-18.

[21]Fazelpour, F., Soltani, N., Nazari, A. and Katal, F., (2015), *Feasibility of satisfying electrical energy needs with wind-photovoltaic-battery hybrid power systems for a household in Qeshm Island Iran*, International Congress Energy and Environmental Engineering and Management Conference, Paris, France.

[22]Karbassi, A., Bidhendi, G.N., Saeedi, M. and Rastegari, A., (2010), *Metals removal during estuarine mixing of Arvand River water with the Persian Gulf water*. Open Geosciences, Vol.2(4), p.531-536.

[23]Moeini, M.H., Etemad-Shahidi, A. and Chegini, V., (2010), *Wave modeling and extreme value analysis off the northern coast of the Persian Gulf*. Applied Ocean Research, Vol.32(2), p.209-218.

[24]Yao, F., (2008), *Water mass formation and circulation in the Persian Gulf and water exchange with the Indian Ocean*. PhD thesis, University of Miami.

[25]Mahmoudov, M., Chegini, V. and Montazeri Namin, M., (2011), *Three-Dimensional Simulation of Qeshm Channel Currents*. Journal of the Persian Gulf, Vol.2(3), p.9-16.

[26]Foreman, M.G.G., (1979), *Manual for tidal heights analysis and prediction*. Pacific Marine Science Report 77-10, Institute of Ocean Sciences, Patricia Bay, Sidney, p.1-97.

[27]Najafi, H.S. and Noye, B.J., (1997), *Modelling tides in the Persian Gulf using dynamic nesting*, PhD thesis, University of Adelaide.

[28]Badri, M.A. and Wilders, P., (2012), *Flow estimation for the Persian Gulf using a kelvin wave expansion*. Indian Journal of Geo-Marine Science, Vol.41(3), p.249-258.

[29]Emami, M., Soyuf Jahromi, M., and Behmanzadegan, A., (2019), *Coastline Effect on Tidal Flow Pattern*. Journal of Marine Science and Technology, Vol.18(2), p.12-25. (In Persian)

[30]Moharir, R.V., Khairnar, K. and Paunikar, W.N., (2014), *MIKE 3 as a modeling tool for flow characterization: A review of applications on water bodies. International Journal of Advanced Studies in Computers*, Science and Engineering, Vol.3(3), p.32-43.

[31]Li, P., Li, G., Qiao, L., Chen, X., Shi, J., Gao, F., Wang, N. and Yue, S., (2014), *Modeling the tidal dynamic changes induced by the bridge in Jiaozhou Bay, Qingdao, China*. Continental Shelf Research, Vol.84, p.43-53.

[32]Kaiser, G., Scheele, L., Kortenhaus, A., Løvholt, F., Römer, H. and Leschka, S., (2011), *The influence of land cover roughness on the results of high resolution tsunami inundation modeling*. Natural Hazards and Earth System Sciences, Vol.11(9), p.2521-2540.

[33] Villaret, C., Hervouet, J.M., Kopmann, R., Merkel, U. and Davies, A.G., (2013), *Morphodynamic modeling using the Telemac finite-element system*. Computers and Geosciences, Vol.53, p.105-113.

[34] Kramer, S.C. and Piggott, M.D., (2016), *A correction to the enhanced bottom drag parameterisation of tidal turbines*. Renewable Energy, Vol.92, p.385-396.

[35]Ershadi, S., Arasteh, M. and Tajziehchi, M., (2013), *Numerical Modeling of Flow Pattern Changes in Tidal Inlet of TIYAB Port*, Research Journal of Environmental and Earth Sciences, Vol.5(11), p.691-702.

[36]Peykanpour, P., Bozorgi, M., Moein, M. and Shamaii, A., (2016), *Tidal currents model of Persian Gulf*, IIOABJ, Vol.7(5), p.293-301.

[37]Radfar, S., Panahi, R., Javaherchi, T., Filom, S. and Mazyaki, A.R., (2017), *A comprehensive insight into tidal stream energy farms in Iran*. Renewable and Sustainable Energy Reviews, Vol.79, p.323-338.

[38]UNESCO (1981) *Tenth report of the joint panel on oceanographic tables and standards.* UNESCO Technical Papers in Marine Science, Vol.36, p.1-28.

[39]DHI., (2009), *MIKE 21 & MIKE 3 Flow Model FM Hydrodynamic and Transport Module – Scientific Documentation*, MIKE by DHI, Horsholm, Denmark.

[40]www.boprc.govt.nz

[41]https://erddap.marine.ie

[42]Edalati, S., Ameri, M. and Iranmanesh, M., (2015), *Estimating and modeling monthly mean daily global solar radiation on horizontal surfaces using artificial neural networks in south east of Iran*, Journal of Renewable Energy and Environment, Vol.2 (1), p. 41-47.

[43]The MathWorks Inc., (2016), *MATLAB and Statistics Toolbox 64-bit*, Version 2016a, Release 2016a, Natick, Massachusetts, USA.

[44]Padman, L., and Erofeeva, S., (2005), *Tide Model Driver (TMD) Manual*. Earth and Space Research. Version 1.2. 28 November 2005.

[45]http://polaris.esr.org/ptm_index.html

[46]Nirwansyah, A. W., & Braun, B. (2019), *Mapping impact of tidal flooding on solar salt farming in Northern Java using a hydrodynamic model*. ISPRS International Journal of Geo-Information, Vol.8(10), p.451.

[47] ftp://ftp.oce.orst.edu/dist/tides/regional/PerS.tar.Z
[48] http://volkov.oce.orst.edu/tides/PerS.html
[49] https://tides4fishing.com/as/iran
[50] Khosravi, M., Siadatmousavi, S.M., Vennell, R. and Chegini, V., (2018), *The transverse dynamics of flow in a tidal channel within a greater strait*. Ocean Dynamics, Vol.68(2), p.239-254.
[51] Wood, D. (2006), MIKE BASIN. DHI water and environment, p.1-38.
[52] Soleimani, K., Ketabdari, M.J. and Khorasani, F., (2015), *Feasibility study on tidal and wave energy conversion in Iranian seas*. Sustainable Energy Technologies and Assessments, Vol.11, p.77-86.
[53] Bryden, I.G., Grinsted, T. and Melville, G.T., (2004), *Assessing the potential of a simple tidal channel to deliver useful energy*. Applied Ocean Research, Vol. 26(5), p.198-204.
[54] Bryden, I.G. and Couch, S.J., (2006), *ME1—marine energy extraction: tidal resource analysis*. Renewable Energy, Vol.31(2), p.133-139.
[55] https://voith.com/corp-en/BulbPitS-Turbines_Generators.pdf
[56] 56- JKP Application Development Services, (2016), *Microsoft Office Excel*, 64-bit, Version 2016, Weert, The Netherlands.